JACS
JOURNAL OF THE AMERICAN CHEMICAL SOCIETY
Article
pubs.acs.org/JACS

All-Inorganic Networks and Tetramer Based on Tin(II)-Containing Polyoxometalates: Tuning Structural and Spectral Properties with Lone-Pairs

Chongchao Zhao, Elliot N. Glass, Bryant Chica, Djamaladdin G. Musaev, Jordan M. Sumliner, R. Brian Dyer, Tianquan Lian, and Craig L. Hill*

Department of Chemistry and Cherry L. Emerson Center for Scientific Computation, Emory University, Atlanta, Georgia 30322, United States

Supporting Information

ABSTRACT: Two MOF-like but all-inorganic polyoxometalate-based networks, $[Na_7X_2W_{18}Sn_9Cl_5O_{68}\cdot(H_2O)_m]_n$ (**1**, X = Si, m = 35; **2**, X = Ge, m = 41), and the molecular tetramer $Na_6[\{Na(\mu\text{-}OH_2)(OH_2)_2\}_6\{Sn_6(B\text{-}SbW_9O_{33})_2\}_2]\cdot 50H_2O$ (**3**) have been prepared and characterized by X-ray diffraction and spectroscopic methods. All three compounds exhibit unique structural features, and networks **1** and **2** incorporate the highest nuclearity of Sn(II)-containing POMs to date. Tetramer **3** comprises bridging Sn(II) ions with $[B\text{-}SbW_9O_{33}]^{9-}$ units and exhibits two highly unusual features, a long-range Sb···Sb interaction and an intramolecular charge-transfer transition involving donation of the lone-pair electron density on both Sb(III) and Sn(II) to the POM. The electronic structure and excited-state dynamics have been studied by transient spectroscopy, spectroelectrochemistry, DFT calculations, and resonance Raman spectroscopy. The synergistic effect of two types of stereoactive lone-pairs on Sb(III) and Sn(II) is critical for the charge-transfer absorption feature in the visible.

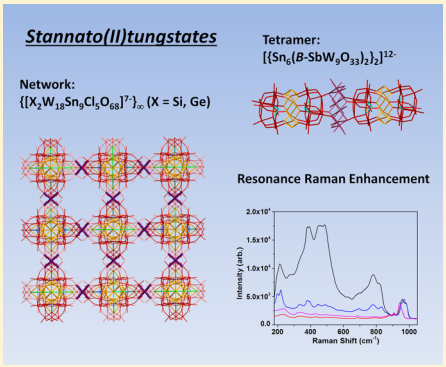

INTRODUCTION

Polyoxometalates (POMs) have been widely studied in context with medicine, magnetism, materials science, and in particular, catalysis.[1−3] POMs cover a wide range of sizes and archetypes, from molecular species to giant wheel/capsule-shaped molecules.[4−9] Recently, like nanoparticles,[10,11] POMs have been introduced into metal−organic framework (MOF) pores for enhanced catalytic and photochemical reactions and in some cases, for MOF stabilization.[12−16] POMs have also been covalently bound to organic linkages to form hybrid molecular cages and frameworks.[17,18] However, purely inorganic molecular metal-oxide networks, for which POMs are ideal candidates, are rare. Although there are a few crystal structures of conventional (d^0) Keggin POMs linked into chains and networks through alkali metal counterions,[19−22] they dissociate upon dissolution and do not exhibit unique photochemical or catalytic properties. Purely POM-based networks containing transition metals are of greater interest because by tuning the electronic properties of the substituted 3d metals, these functional networks can integrate the versatile catalytic and photocatalytic activities of POMs within the structural features of MOFs.[23,24] Cronin *et al.* have pioneered some carbon-free POM-linked structures and recently reported a network comprising Mn(II)-linked $[P_8W_{48}O_{184}]^{40-}$ units that exhibits unique electrochemical behavior.[25,26]

Nonbonding valence electron pairs, lone-pairs, as often observed in p-block elements, play a significant role in structural chemistry, catalysts, and semiconductors.[27−29] In POMs with pyramidal heteroanions, stereochemically active lone-pair electrons frequently influence the structural features, as seen in some Sb(III)-, Bi(III)-, and As(III)-centered derivatives.[30−37] The lone-pair-bearing p-block metals, i.e., Sn(II), can exist as internal heteroatoms or external metal centers, and the latter offers the potential for further coordination to a secondary building unit (SBU) to form high dimensional structures. However, so far this behavior has not been observed in Sn(II)-containing POMs.[38−43] More recently, photochemical properties of a stannato(II)tungstate have been reported, but this study lacks insightful electronic delineation.[43] Inspired by the above observations, we report here two all-inorganic MOF-like Sn(II)-substituted POMs: $[Na_7X_2W_{18}Sn_9Cl_5O_{68}\cdot(H_2O)_m]_n$ (**1**, X = Si, m = 35; **2**, X = Ge, m = 41) and the compositionally similar tetrameric compound $Na_6[\{Na(\mu\text{-}OH_2)(OH_2)_2\}_6\{Sn_6(B\text{-}SbW_9O_{33})_2\}_2]\cdot 50H_2O$ (**3**). Compound **3** contains two types of stereoactive lone-pairs. Each of these compounds displays unique structural features, and a range of techniques identify the nature and excited state dynamics of the unusual intramolecular charge-transfer absorption in **3**.

Received: June 16, 2014
Published: July 30, 2014

   dx.doi.org/10.1021/ja5060127 | J. Am. Chem. Soc. 2014, 136, 12085−12091

Table 1. Crystal Structure Data for Compounds 1, 2, and 3

	1	2	3
empirical formula	$H_{70}O_{103}Cl_5Na_7Si_2Sn_9W_{18}$	$H_{82}O_{109}Cl_5Na_7Ge_2Sn_9W_{18}$	$H_{136}O_{200}Na_{12}Sb_4Sn_{12}W_{36}$
T [K]	173(2)	173(2)	173(2)
M_r [g mol^{-1}]	6499.99	6695.94	12156.60
crystal system	tetragonal	tetragonal	trigonal
space group	$P42/ncm$	$P42/ncm$	$R\bar{3}m$
a [Å]	21.438(4)	21.416(3)	17.778(5)
b [Å]	21.438(4)	21.416(3)	17.778(5)
c [Å]	23.126(4)	23.133(3)	45.221(13)
V [Å^3]	10629(3)	10610(2)	12378(6)
Z	4	4	6
ρ_{calcd} [g cm^{-3}]	3.696	3.758	4.598
μ [mm^{-1}]	21.697	22.268	27.546
reflections collected	93868	58692	12880
independent refl (R_{int})	5454 (0.1042)	5861 (0.0895)	3350 (0.1171)
goodness-of-fit	1.151	1.177	0.998
$R_1{}^a$ [$I > 2\sigma(I)$]	0.0685	0.0666	0.0680
$wR_2{}^a$	0.1550	0.1043	0.1204
largest diff peak and hole [e Å^3]	3.729, −2.737	2.343, −1.950	5.875, −4.457

$^a R_1 = \Sigma \, ||F_o| - |F_c||/\Sigma|F_o|$. $wR_2 = \{\Sigma[w(F_o^2 - F_c^2)^2/\Sigma w(F_o^2)^2]\}^{1/2}$.

EXPERIMENTAL SECTION

Materials and Methods. All chemicals were reagent grade and used as supplied. The trivacant POM precursors $Na_{10}[\alpha\text{-}SiW_9O_{34}]\cdot nH_2O$, $Na_{10}[\alpha\text{-}GeW_9O_{34}]\cdot nH_2O$, and $Na_9[B\text{-}SbW_9O_{33}]\cdot nH_2O$ were prepared according to reported methods.[30,44,45] Their purities were determined through FT-IR spectroscopy. UV−vis absorption spectra were acquired using an Agilent 8453 spectrophotometer equipped with a diode-array detector and an Agilent 89090A cell temperature controller unit. The FT-IR spectra were measured on a Thermo Nicolet 6700 spectrometer with KBr pellets (2%). Elemental analyses were performed by Galbraith Lab Inc., Knoxville, TN. Thermogravimetric analysis was acquired on a Perkin Elmer STA 6000 analyzer.

Synthesis of 1. $Na_{10}[\alpha\text{-}SiW_9O_{34}]\cdot 23H_2O$ (1.6 g, 0.6 mmol) was dissolved in 20 mL of H_2O, followed by addition of 1.0 M HCl until the pH was ∼6.7. $SnCl_2\cdot 2H_2O$ (285 mg, 1.25 mmol) was added to the above solution quickly. The solution immediately turned orange and some unidentified white precipitate formed, with the pH decreasing to 2.0. NaCl (400 mg) was then added. The mixtures were heated to 70 °C for 30 min and then cooled to room temperature and filtered. Orange needle-shape crystals were obtained after slow evaporation within a week. Yield: 430 mg (47% based on Sn). FTIR (1100−500 cm^{-1}; 2% KBr pellets): 996 (m), 948 (m), 890 (s), 786 (m), 687 (s), 646 (m), 532 (w). Anal. Calcd for $H_{70}O_{103}Cl_5Na_7Si_2Sn_9W_{18}$: Cl, 2.7; Na, 2.5; Si, 0.86; Sn, 16.5; W, 51.0. Found: Cl, 2.5; Na, 2.4; Si, 0.84; Sn, 15.5; W, 49.6. TGA: weight loss, 9.7% (30−500 °C; "$35H_2O$") and 2.7% (500−700 °C; "5Cl").

Synthesis of 2. This complex was prepared using a procedure similar to that for **1** above except that $Na_{10}[\alpha\text{-}GeW_9O_{34}]\cdot nH_2O$ (1.7 g, 0.6 mmol) was used. Yield: 370 mg (40% based on Sn). FTIR (1100−500 cm^{-1}; 2% KBr pellets): 945 (m), 880 (s), 797 (s), 683 (s), 639 (m), 526 (w). Anal. Calcd for $H_{82}O_{109}Cl_5Na_7Ge_2Sn_9W_{18}$: Cl, 2.7; Na, 2.4; Ge, 2.2; Sn, 16.0; W, 49.5. Found: Cl, 2.3; Na, 2.2; Ge, 1.9; Sn, 15.1; W, 48.1. TGA: weight loss, 11.0% (30−500 °C; "$41H_2O$") and 2.7% (500−700 °C; "5Cl").

Synthesis of 3. $Na_9[B\text{-}SbW_9O_{33}]\cdot nH_2O$ (1.6 g, 0.6 mmol) was dissolved in 0.5 M NaCl solution. The pH was then adjusted to ∼6.5 by adding 1.0 M HCl. $SnCl_2\cdot 2H_2O$ (285 mg, 1.25 mmol) was added, and the mixture was heated at 70 °C for 15 min. The solution was then filtered and allowed to slowly evaporate. Red crystals were obtained within 2 days. Yield: 370 mg (40% based on Sn). FTIR (1100−500 cm^{-1}; 2% KBr pellets): 943 (s), 905 (m), 857 (m), 789 (s), 718 (s), 667 (s). Electronic spectra data (350−700 nm): $\varepsilon_{400\ nm}$ ∼1.05×10^4 M$^{-1}\cdot$cm^{-1}. Anal. Calcd for $H_{136}O_{200}Na_{12}Sb_4Sn_{12}W_{36}$: Na, 2.3; Sb, 4.0; Sn, 11.7; W, 54.5. Found: Na, 2.2; Sb, 3.7; Sn, 11.2; W, 55.0. TGA: weight loss, 7.3% (30−500 °C; "$50H_2O$").

X-ray Crystallography. X-ray analysis was performed on a Bruker D8 SMART APEX CCD sealed tube diffractometer. Diffraction intensities were measured using graphite monochromated Mo Kα radiation (λ = 0.71073 Å) at 173(2) K. Data collection, indexing, and initial cell refinements were carried out by using SMART; frame integration and final cell refinements were accomplished by SAINT.[46] A multiple absorption correction including face indexing was done by SADABS.[47] The molecular structures were determined by direct methods and Fourier techniques and refined by full-matrix least squares. Structure solution and refinement were accomplished using SHELXTL-97.[48] The crystallographic data are summarized in Table 1.

Raman Spectroscopy. Raman spectra were taken using excitation at the 514.5 nm line of an Ar$^+$ ion laser (Spectra Physics) and the 632.8 nm line from a He−Ne laser. Samples were held in NMR tubes and illuminated in a 135° geometry. Scattered light was collected by a 20X microscope objective (Olympus). Scattered excitation light was rejected by supernotch holographic filters (Kaiser Optical), and the Raman scattered light was focused on the entrance slit of a Holo-spec f/1.8 imaging spectrograph (Kaiser Optical) and dispersed on a Pixis 400 CCD camera (Princeton Instruments). Data acquisition was controlled by custom LabView software. Integration times were adjusted to utilize a reasonable amount of the CCD dynamic range (between 0.5 and 5 s). Photostability and lack of sample degradation was confirmed by noting a lack of change in the Raman spectra even under prolonged illumination conditions at increased laser power.

Transient Spectral and Kinetic Analysis. The femtosecond transient absorption spectrometer is based on a regeneratively amplified Ti:sapphire laser system (coherent Legend, 800 nm, 150 fs, 3 mJ/pulse, and 1 kHz repetition rate) and a Helios spectrometer (Ultrafast Systems LLC). The instrument has been described in detail elsewhere.[49,50] The sample (compound **3**) was converted to the tetrabutylammonium salt and dissolved in acetonitrile for transient measurements.

Electrochemistry and Spectroelectrochemistry. Cyclic voltammograms (CVs) of **3** were obtained at room temperature using a BAS CV-50W potentiostat with a standard three-electrode configuration. A glassy-carbon electrode was used as the working electrode. The reference and counter electrodes were Ag/AgCl (3 M NaCl) (BASi) and a platinum wire, respectively. All reported reduction potentials are relative to this reference electrode. CVs were performed in 20 mM sodium acetate buffer (pH = 4) with 0.4 M LiCl as a supporting electrolyte. Visible-light spectroelectrochemical experi-

dx.doi.org/10.1021/ja5060127 | J. Am. Chem. Soc. 2014, 136, 12085−12091

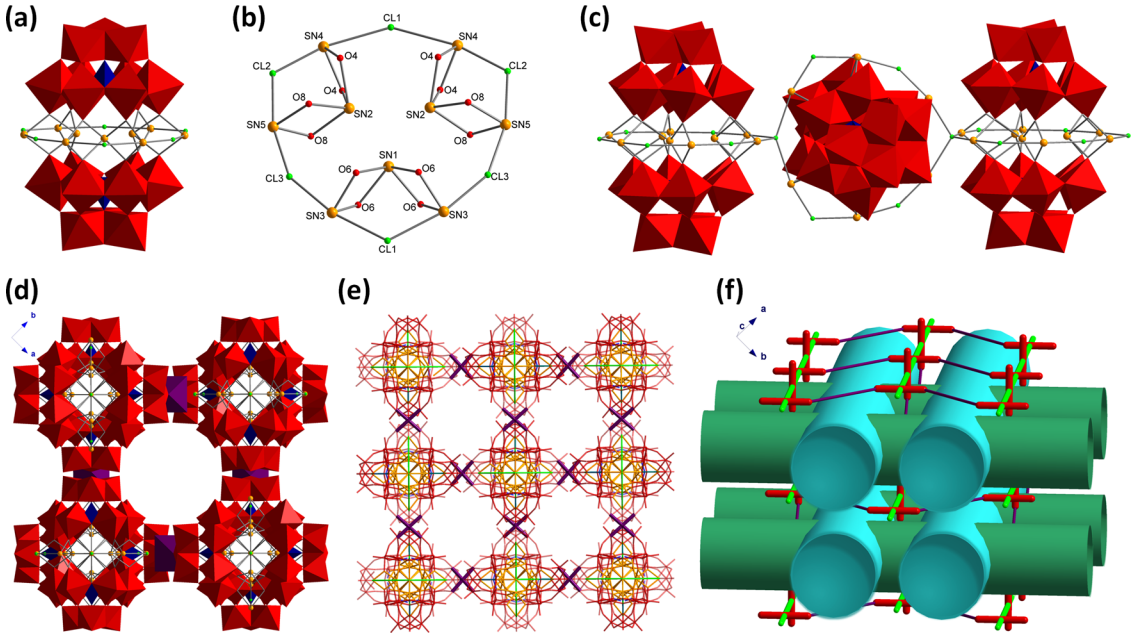

Figure 1. (a) X-ray structure of a single polyanion unit of **1** in combined bond-and-stick and polyhedral notation. Code: Cl, green; Sn, orange; SiO_4, blue; WO_6, red. (b) Representation of the nine Sn(II) centers. (c) 1D chain through μ_4-Cl centers. (d) Porous channels along *c*-axis in **1**. (e) The 3D open framework of **1** shown in stick notation. (f) A topological representation of **1**. The channels are shown as blue/green tubes. The red sticks and green sticks represent a single POM unit and the bridging chloride centers, respectively.

ments were performed with a BASi CV-50W potentiostat, in an ALS SEC-2F spectroelectrochemical flow cell (0.5 mm path length) equipped with an Ocean Optics USB2000+ spectrometer and an LS-1 tungsten lamp. The working electrode was an FTO-coated glass slide, the reference electrode was Ag/AgCl in 3 M NaCl (BASi), and the auxiliary electrode was a stainless steel tube. Ocean Optics Spectrasuite software was used to record the visible spectra and collect absorbance versus time measurements at applied potentials.

Computational Studies. Geometries of the polyanion **3** were optimized, both in the gas phase and in implicit water solution, with no geometric constraints, at its ground singlet state (Supplementary Table S2). In these calculations, we used the DFT method (M06L functional)[51] in conjunction with the split-valence 6-31G(d) basis sets for oxygens and lanl2dz basis sets and associated ECPs for the W, Sb, and Sn atoms,[52−54] which below are referred to as M06L/[lanl2dz +6-31G(d,p)]. The solvent effects were approximated by the polarizable continuum model (PCM)[55,56] employing the UFF radii[57] for all atoms. The above calculations were carried out with the Gaussian 09 software package.[58]

RESULTS AND DISCUSSION

Structural Description. Compounds **1** and **2** both exhibit porous architectures reminiscent of MOFs. The repeating unit of **1** and the Sn(II) centers are shown in Figure 1a and b, respectively. Figure 1c shows the μ_4-Cl bridges that reside in tetrahedral positions with Sn−Cl−Sn angles (*trans*) of 116.5° and 142.6°. Each repeating unit of **1** is perpendicular to its two neighbors forming a one-dimensional (1D) chain. To our knowledge, Cl-bridged 1D POM chains have not been reported previously. Each 1D chain is bound to the four identical proximal chains through $[Na(H_2O)_4]^+$ ions. The *P*42/*ncm* space group dictates that the symmetry-equivalent 1D chains assemble around the 4-fold axis to generate an internal porous channel along the *c*-axis. The channel diameter is ∼9.2 Å estimated from the boundary oxygen nuclei (Figure 1d and e). Another channel with a diameter of 6.1 Å, defined between the edge chloride atoms, is present along the [110] direction (Supplementary Figure S3; Supporting Information). The accessible void space of the 3D channels is ∼28.0% of the unit cell volume (PLATON/SOLV).[59]

The polyanion unit of **1** (D_{3h} symmetry) consists of two [α-SiW_9O_{34}]$^{10-}$ units linked by nine Sn(II) centers. Bond valence sum (BVS) calculations of all nine Sn(II) centers range from 1.75 to 1.98, indicating the low oxidation state (Supplementary Table S1). The structure can be viewed as a typical sandwich motif $\{Sn_3(XW_9)_2\}$, as seen in $[Sn_3(SiW_9O_{34})_2]^{14-}$,[38] surrounded by a 12-membered $\{Sn_6Cl_6\}$ ring in the belt position (Figure 1b). The inner Sn(II) ions display a SnO_4 seesaw molecular geometry with Sn−O distances from 2.25 to 2.29 Å and O−Sn−O angles from 114.5° to 115.9° (O_{ax}−Sn−O_{ax}, O_{eq}−Sn−O_{eq}; ax = axial, eq = equatorial) and 69.6° to 77.4° (O_{ax}−Sn−O_{eq}), respectively. The lone-pairs on Sn(II) occupy the third equatorial position and point toward the central C_3 axis.

The $\{Sn_6Cl_6\}$ ring in the polyanion of **1** encircles $[Sn_3(SiW_9O_{34})_2]^{14-}$ through Sn−O−Sn bonds with angles of 106.2−107.3°. The external Sn(II) centers reside in SnO_2Cl_2 building blocks, which display a seesaw geometry with two chlorides in axial positions and two oxygens in equatorial positions, respectively. The external lone-pairs face away from C_3 axis. The Cl−Sn−Cl bond angles are 165.5−166.5°, while O−Sn−O angles are 74.6−75.3°. The Sn−O bond distances are 2.12−2.15 Å, while Sn−Cl bonds show long distances ranging from 2.68 to 3.18 Å. The Sn−(μ_2-Cl)−Sn linkages are shorter than the Sn−(μ_4-Cl)−Sn linkages.[60,61]

$[\{Na(\mu\text{-}OH_2)(OH_2)_2\}_6\{Sn_6(B\text{-}SbW_9O_{33})_2\}_2]^{6-}$ (the polyanion of **3**) is a tetramer constructed of two $[Sn_6(B\text{-}SbW_9O_{33})_2]^{6-}$ units linked to each other through a polymeric cation, $[Na_6(\mu\text{-}OH_2)_6(OH_2)_{12}]^{6+}$ (Figure 2a and b). $[Sn_6(B\text{-}SbW_9O_{33})_2]^{6-}$ comprises two $[B\text{-}SbW_9O_{33}]^{9-}$ ligands joined by six Sn(II) centers, a structural motif similar to that in $[Sn_6(SnW_9O_{33})_2]^{8-}$.[42] Complex **3** (with a D_{3d} polyanion) crystallizes in the trigonal $R\bar{3}m$ space group (Figure 2c) and has one $[B\text{-}SbW_9O_{33}]^{9-}$ unit rotated by 60° relative to the other.

dx.doi.org/10.1021/ja5060127 | J. Am. Chem. Soc. 2014, 136, 12085−12091

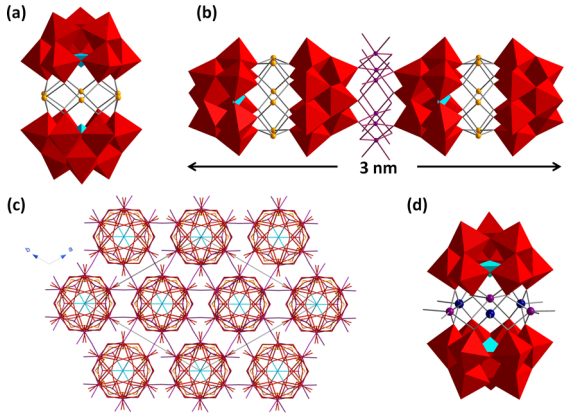

Figure 2. (a) X-ray structure of $[Sn_6(B\text{-}SbW_9O_{33})_2]^{6-}$ in combined bond-and-stick and polyhedral notation. Code: Sb, cyan (other colors as in Figure 1). (b) A "double-sandwich" structure of **3** involving a hexa-Na^+ polycation. (c) The arrangement of **3** polyanions along the *c*-axis (stick notation). (d) X-ray structure of an analogous structure, $[\{Co(H_2O)\}_3\{Na(H_2O)_2\}_3(B\text{-}SbW_9O_{33})_2]^{9-}$ (**CoPOM**). Code: Co, blue; Na, purple.

The Sn–O bonds range from 2.25 to 2.29 Å. Each Sn(II) is four-coordinated and in the +2 oxidation state (Supplementary Table S1). The Sn–O–Sn bond angles are 107.8–109.5°, and the O–Sn–O angles are 118.1–118.7° (O_{ax}–Sn–O_{ax}, O_{eq}–Sn–O_{eq}) and 70.4–79.7° (O_{ax}–Sn–O_{eq}), respectively. Each Na^+ ion in $[Na_6(\mu\text{-}OH_2)_6(OH_2)_{12}]^{6+}$ resides in an octahedral environment with Na–O bond distances of 2.24–2.26 Å (terminal) and 2.43–2.49 Å (bridged), respectively. This nanosized cluster has a length of ca. 3 nm.

Electronic Absorption Spectra, Electrochemistry, and Spectroelectrochemical Measurements. Network solids are generally not soluble, and that is the case with **1** and **2**. The compounds are colored (**1** and **2** are orange and **3** is red) in the solid state. As seen in Figure 3a and b, the UV–vis absorption spectrum of **3** shows a broad band in the visible region extending to about 650 nm ($\varepsilon_{400\ nm}$: 1.05 × 10^4 $M^{-1}\cdot cm^{-1}$). The $SnCl_2$ and POM ligand precursors, unlike **1**–**3**, are both colorless; consequently, this absorption feature is likely due to a transition involving lone-pair donors (could be located on Sn(II) and Sb(III) centers) and POM acceptors. Significantly, this p-block-element-to-POM electronic structure is distinct from the metal-to-polyoxometalate (MPCT) transitions in two recent reports because the latter involve donation of d electron density on the donor site, e.g., Re(I), to the delocalized POM multimetal orbitals.[49,62,63] Particularly, the presence of lone-pairs in **1**–**3** contributes to a large local dipole moment, which has been shown to facilitate electron–hole charge separation.[64–66]

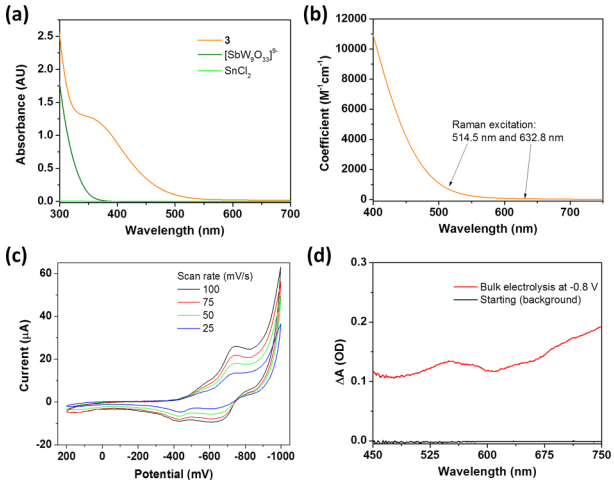

Figure 3. (a) Normalized electronic absorption spectra of **3**, $[B\text{-}SbW_9O_{33}]^{9-}$ (2 equiv) and $SnCl_2$ (6 equiv) in aqueous solution (pH = 1). (b) UV–vis absorption spectrum of **3**. The arrows indicate the wavelengths used for Raman excitation. (c) Cyclic voltammograms of **3** at different scan rates in the range of +0.2 to −1.0 V vs Ag/AgCl. (d) Ground state UV–vis absorption difference spectra of reduced **3** (generated at −0.8 V vs Ag/AgCl) in sodium acetate buffer.

As shown in Figure 3c, in the negative potential domain, the CVs of **3** display two quasi-reversible poorly resolved peaks with a nearly 1:1 current ratio, which is consistent with two one-electron transfer processes ($E_{1/2}$ at *ca.* −0.48 and −0.65 V, respectively). These patterns are similar to those of $[B\text{-}SbW_9O_{33}]^{9-}$ derivatives.[67,68] The width of the CV peaks is consistent with slow electron transfer processes, likely due to high reorganization energies in **3**. The peaks in the negative domain are assigned to W(VI)/W(V) reductions. The peaks for the Sn(II)-centered redox processes do not show up in the CV scans. The spectroelectrochemical absorption spectra for reduced **3** in the ground state were recorded at an applied potential of −0.80 V vs Ag/AgCl. As seen in Figure 3d, a new absorption band from ca. 550 nm to the near-IR was observed, which is a characteristic feature of reduced POMs, the "heteropoly blues".[69] These new absorption features can be attributed to W(V) d-d and W(V)–W(VI) intervalence charge transfer (IVCT) transitions in reduced POMs.[70,71] Compound **3** shows good reversibility in spectroelectrochemical measurements, where bulk reduction and air-based reoxidation processes can be repeated sequentially. CVs were not collected for **1** or **2** due to poor solubility.

Computational Studies. Compound **3**, unlike **1** and **2**, contains Sb(III) lone-pairs in addition to the Sn(II) lone-pair electrons and exhibits an extraordinarily high extinction coefficient in the visible region. In order to understand the origin of these intense transitions (absorptions), we investigated the geometrical and electronic structure of **3** using computational methods. The calculated Sn–O bond distances of the central hexanuclear Sn(II) "belt" range from 2.21 to 2.23 Å, the Sn–O–Sn bond angles are 107.1–107.8°, the W–O(Sn) bond distances are within 1.94–1.95 Å, and the Sb–O bond distances (symmetrically equivalent) are 2.01 Å. These geometric parameters are in excellent agreement with the experimental values.

Interestingly, the frontier orbital analyses of the singlet ground state indicate the existence of a weak Sb···Sb interaction in **3**: the calculated energy difference between the Sb–Sb bonding (HOMO-8) and Sb–Sb antibonding (HOMO-7) orbitals is only 0.33 eV (Figure 4). This is likely due to long-range lone-pair interaction.[72] The first six HOMOs of **3** are lone-pairs on the Sn centers, which are clustered within a 0.30 eV energy range. The next orbitals are primarily Sb–Sb and Sb–O in nature and doubly occupied. The leading LUMOs are mostly W-centered orbitals. The calculated HOMO–LUMO energy gap is 1.67 eV. Since single-electron transfer from HOMO to LUMO leads to a triplet state with a multi-determinant wave function, our calculations of the triplet state failed to converge; at this time we cannot report a reliable singlet–triplet energy splitting.

dx.doi.org/10.1021/ja5060127 | J. Am. Chem. Soc. 2014, 136, 12085–12091

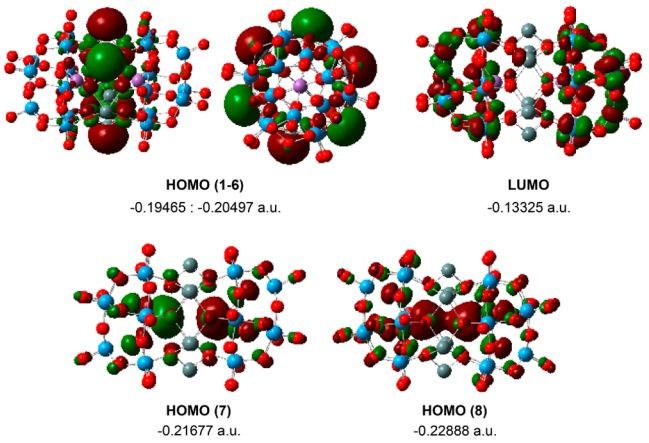

Figure 4. Several highest occupied (HOMO) and lowest unoccupied (LUMO) orbitals and their orbital energies (in Hartree) in complex **3**.

Resonance Raman Spectroscopy. Resonance Raman (RR) spectroscopy has also been used to characterize the putative lone-pair-to-POM charge-transfer transition in **3**. The RR spectra of **3** as well as $Na_9[B\text{-}SbW_9O_{33}]$, the colorless precursor, and $Na_9[\{Co(H_2O)\}_3\{Na(H_2O)_2\}_3(B\text{-}SbW_9O_{33})_2]$ (**CoPOM**; structure shown in Figure 2d),[73,74] a known complex with a $\{Co_3Na_3\}$ belt similar to $\{Sn_6\}$ in **3**, were all compared. Although detailed assignment of the vibrational spectra is beyond the scope of this work, conclusions can be drawn from the data. Two Raman probe wavelengths were used, 514.5 and 632.8 nm, enabling a simple two-point excitation profile to be observed (Figure 3b). As shown in Figure 5a and b, upon changing the excitation wavelength from 632.8 nm ($\varepsilon \sim 55\ M^{-1}\ cm^{-1}$ for **3**) to 514.5 nm ($\varepsilon \sim 710\ M^{-1}\ cm^{-1}$ for **3**), there is a significant increase in relative intensity of several transitions in the low-frequency region (300–400 cm^{-1}), where mostly M–O stretching and O–M–O (M = Sb or Sn) bending modes are expected due to a large degree of coupling in the highly symmetric Sn cluster, and in the region of ~800 cm^{-1} where W–O–M bending modes reside.[36,39,75−77] Specifically, the vibration at 487 cm^{-1} present in both **3** and $Na_9[B\text{-}SbW_9O_{33}]$ exhibits little perturbation upon complexation of the $\{Sn_6\}$ cluster but gains great resonance enhancement upon excitation. This vibration can be assigned to a localized mode in the $[B\text{-}SbW_9O_{33}]^{9-}$ polyanion, which likely has both W–O and Sb–O character. Similarly the vibration at 627 cm^{-1}, which can be observed as a weak mode in $Na_9[B\text{-}SbW_9O_{33}]$, gains comparable intensity to the nearby 690 cm^{-1} mode upon 514.5 nm excitation. Various other enhanced vibrations, such as the band at 825 cm^{-1}, likely a W–O–Sn stretching mode,[39] arise only after the formation of the $\{Sn_6\}$ cluster, indicating either local Sn–O modes or coupling of POM modes to the $\{Sn_6\}$ core. This observation of resonantly enhanced vibrations attributable to both local POM modes and modes coupled to the central $\{Sn_6\}$ cluster supports the assignment as a charge transfer transition. There is, however, no comparable enhancement trend for **1** or **2** (Figure 5b and Supplementary Figure S4) despite a similar (although weaker) visible absorption. This observation supports the important role of Sb(III) and the unique structure of the central $\{Sn_6\}$ cluster in the charge-transfer transition. There is also no enhancement of lower frequency bands for **CoPOM**, although it has a similar geometry to **3** and exhibits d-d bands in the visible region that principally involve five-coordinate Co(II) ions (Figure 2d and Supplementary Figure S5). This excludes the enhancement being a result of the geometric motif of the core atoms. Shifts in the redox potentials and energy levels of the POM LUMOs arising from different heteroatoms can account for some of the discrepancy of photoactivity for the three stannato(II)-tungstates.[78−80] The collective results indicate that the synergistic effect of Sn(II) and Sb(III) lone-pairs account for the particular charge-transfer characteristics in **3**.

Transient Absorption Spectroscopy. Femtosecond visible pump–probe spectroscopy was used to study the kinetics of this lone-pair-to-POM transition. Upon photoexcitation (at 400 nm) the transient absorption spectra show a new species with a broad absorption from ~500 nm to near-IR (Figure 5c). The new absorption feature is reminiscent of the UV–vis absorption spectrum of an electrochemically reduced **3** (Figure 3d), the result of the photoexcited electron residing in the delocalized POM acceptor orbitals. Differences between the two spectra are expected on the basis that the photoexcited species contains a transiently oxidized donor that cannot be replicated electrochemically. The kinetics are monitored at 520 and 720 nm, respectively, and fitted by a multiexponential function. An instantaneous formation of the excited states and a biexponential decay was documented. There is a long-lived component at 720 nm that persists with a time constant of 66 ps. This component has a shallow, broad absorbance that has a heteropoly blue spectral signature (Supplementary Figure S6 and Table S3).[81−83] These results, combined with the above HOMO/LUMO assignment, suggest a transition from lone-pair donors to POM acceptors upon excitation; however, this

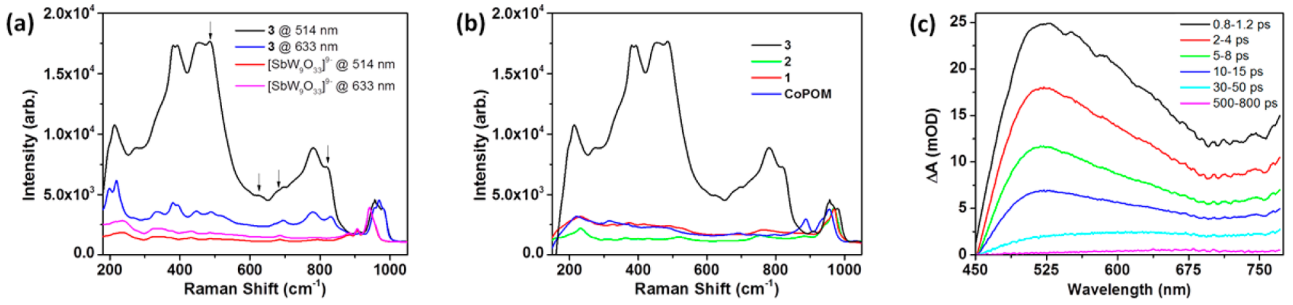

Figure 5. (a) RR spectra of **3** and $[B\text{-}SbW_9O_{33}]^{9-}$ acquired at two excitation wavelengths. Spectra are normalized to the intensity of the highest energy W–O stretch (~950–990 cm^{-1}). Rapid falloff of intensity at energies lower than ~200 cm^{-1} is due to the bandwidth of the holographic notch filter. Arrows indicate the representative modes discussed above (487, 627, 690, and 825 cm^{-1}, respectively). (b) Normalized RR spectra of **1**, **2**, **3**, and **CoPOM** at 514 nm excitation. (c) Average visible transient absorption spectra of TBA-**3** (TBA = tetrabutylammonium) in acetonitrile at indicated delay time windows after 400 nm excitation.

dx.doi.org/10.1021/ja5060127 | J. Am. Chem. Soc. 2014, 136, 12085–12091

does not exclude the possible contribution of LMCT (oxygen-to-tungsten) transitions in the transient spectra.

CONCLUSIONS

Structural and spectral features of Sn(II)-containing POMs, networks **1** and **2** and the molecular compound **3**, have been thoroughly investigated. The external lone-pairs of Sn(II) in **1** and **2** direct the formation of high dimensional structures. The coexistence of Sb(III)/Sn(II) lone-pair electrons lead to a synergistic effect contributing to the charge-transfer absorption features of **3**. This study broadens the frontier of POM chemistry in the context of self-assembly and energy conversion, especially for the lesser-documented p-block element POM families.

ASSOCIATED CONTENT

Supporting Information

Crystallographic information for complexes **1**−**3** in CIF format and additional figures and tables for structural, spectral, and computational characterization. This material is available free of charge via the Internet at http://pubs.acs.org.

AUTHOR INFORMATION

Corresponding Author

chill@emory.edu

Notes

The authors declare no competing financial interest.

ACKNOWLEDGMENTS

This work was funded by the U.S. Department of Energy Office of Basic Energy Sciences, Solar Photochemistry Program (DE-FG02-07ER-15906) to C.L.H., T.L., and D.G.M. The authors also gratefully acknowledge NSF MRI-R2 instrument grant (CHE-0958205) and use of resources at Cherry Emerson Center for Scientific Computation.

REFERENCES

(1) *Polyoxometalates: From Platonic Solids to Anti-retroviral Activity*; Pope, M. T., Müller, A., Eds.; Kluwer Academic Publishers: Dordrecht, The Netherlands, 1993.
(2) Miras, H. N.; Yan, J.; Long, D.-L.; Cronin, L. *Chem. Soc. Rev.* **2012**, *41*, 7403.
(3) Lv, H.; Geletii, Y. V.; Zhao, C.; Vickers, J. W.; Zhu, G.; Luo, Z.; Song, J.; Lian, T.; Musaev, D. G.; Hill, C. L. *Chem. Soc. Rev.* **2012**, *41*, 7572.
(4) Müller, A.; Shah, S. Q. N.; Bogge, H.; Schmidtmann, M. *Nature* **1999**, *397*, 48.
(5) Mal, S. S.; Kortz, U. *Angew. Chem., Int. Ed.* **2005**, *44*, 3777.
(6) Bassil, B. S.; Dickman, M. H.; Römer, I.; von der Kammer, B.; Kortz, U. *Angew. Chem., Int. Ed.* **2007**, *46*, 6192.
(7) Müller, A.; Serain, C. *Acc. Chem. Res.* **2000**, *33*, 2.
(8) Schäffer, C.; Merca, A.; Bögge, H.; Todea, A. M.; Kistler, M. L.; Liu, T.; Thouvenot, R.; Gouzerh, P.; Müller, A. *Angew. Chem., Int. Ed.* **2009**, *48*, 149.
(9) Botar, B.; Kögerler, P.; Hill, C. L. *J. Am. Chem. Soc.* **2006**, *128*, 5336.
(10) Lee, J. Y.; Farha, O. K.; Roberts, J.; Scheidt, K. A.; Nguyen, S. B. T.; Hupp, J. T. *Chem. Soc. Rev.* **2009**, *38*, 1450.
(11) Wang, C.; deKrafft, K. E.; Lin, W. *J. Am. Chem. Soc.* **2012**, *134*, 7211.
(12) Nohra, B.; El Moll, H.; Rodriguez-Albelo, L. M.; Mialane, P.; Marrot, J. é.; Mellot-Draznieks, C.; O'Keeffe, M.; Ngo Biboum, R.; Lemaire, J.; Keita, B.; Nadjo, L.; Dolbecq, A. *J. Am. Chem. Soc.* **2011**, *133*, 13363.
(13) Song, J.; Luo, Z.; Britt, D.; Furukawa, H.; Yaghi, O. M.; Hardcastle, K. I.; Hill, C. L. *J. Am. Chem. Soc.* **2011**, *133*, 16839.
(14) Zheng, S.-T.; Zhang, J.; Yang, G.-Y. *Angew. Chem., Int. Ed.* **2008**, *47*, 3909.
(15) Ma, F.-J.; Liu, S.-X.; Sun, C.-Y.; Liang, D.-D.; Ren, G.-J.; Wei, F.; Chen, Y.-G.; Su, Z.-M. *J. Am. Chem. Soc.* **2011**, *133*, 4178.
(16) Juan-Alcañiz, J.; Goesten, M. G.; Ramos-Fernandez, E. V.; Gascon, J.; Kapteijn, F. *New J. Chem.* **2012**, *36*, 977.
(17) Zheng, S.-T.; Zhang, J.; Li, X.-X.; Fang, W.-H.; Yang, G.-Y. *J. Am. Chem. Soc.* **2010**, *132*, 15102.
(18) Zhang, L.; Schmitt, W. *J. Am. Chem. Soc.* **2011**, *133*, 11240.
(19) Bonfim, R. d. P. F.; Moura, L. C. d.; Pizzala, H.; Caldarelli, S.; Paul, S.; Eon, J. G.; Mentré, O.; Capron, M.; Delevoye, L.; Payen, E. *Inorg. Chem.* **2007**, *46*, 7371.
(20) Han, X.-B.; Zhang, Z.-M.; Wang, Z.-S.; Zhang, H.; Duan, H.; Wang, E.-B. *Inorg. Chem. Commun.* **2012**, *18*, 47.
(21) Gao, S.; Cao, R.; Bi, W.; Li, X.; Lin, Z. *Microporous Mesoporous Mater.* **2005**, *80*, 139.
(22) Mothé-Esteves, P.; Pereira, M. M.; Arichi, J.; Louis, B. *Cryst. Growth Des.* **2009**, *10*, 371.
(23) Liu, D.; Lu, Y.; Tan, H.-Q.; Chen, W.-L.; Zhang, Z.-M.; Li, Y.-G.; Wang, E. *Chem. Commun.* **2013**, *49*, 3673.
(24) Li, F.; Meng, F.; Ma, L.; Xu, L.; Sun, Z.; Gao, Q. *Dalton Trans.* **2013**, *42*, 12079.
(25) Streb, C.; Ritchie, C.; Long, D.-L.; Kögerler, P.; Cronin, L. *Angew. Chem., Int. Ed.* **2007**, *46*, 7579.
(26) Mitchell, S. G.; Streb, C.; Miras, H. N.; Boyd, T.; Long, D.-L.; Cronin, L. *Nat. Chem.* **2010**, *2*, 308.
(27) Sato, J.; Kobayashi, H.; Inoue, Y. *J. Phys. Chem. B* **2003**, *107*, 7970.
(28) Walsh, A.; Payne, D. J.; Egdell, R. G.; Watson, G. W. *Chem. Soc. Rev.* **2011**, *40*, 4455.
(29) Brown, D. *J. Phys. Chem. A* **2011**, *115*, 12638.
(30) Bosing, M.; Loose, I.; Pohlmann, H.; Krebs, B. *Chem.—Eur. J.* **1997**, *3*, 1232.
(31) Sazani, G.; Dickman, M. H.; Pope, M. T. *Inorg. Chem.* **2000**, *39*, 939.
(32) Bi, L.-H.; Al-Kadamany, G.; Chubarova, E. V.; Dickman, M. H.; Chen, L.; Gopala, D. S.; Richards, R. M.; Keita, B.; Nadjo, L.; Jaensch, H.; Mathys, G.; Kortz, U. *Inorg. Chem.* **2009**, *48*, 10068.
(33) Zhao, C.; Kambara, C. S.; Yang, Y.; Kaledin, A. L.; Musaev, D. G.; Lian, T.; Hill, C. L. *Inorg. Chem.* **2013**, *52*, 671.
(34) Corella-Ochoa, M. N.; Miras, H. N.; Kidd, A.; Long, D.-L.; Cronin, L. *Chem. Commun.* **2011**, *47*, 8799.
(35) Tsunashima, R.; Long, D.-L.; Endo, T.; Noro, S.-i.; Akutagawa, T.; Nakamura, T.; Cabrera, R. Q.; McMillan, P. F.; Kögerler, P.; Cronin, L. *Phys. Chem. Chem. Phys.* **2011**, *13*, 7295.
(36) Cabrera, R. Q.; Firth, S.; Blackman, C. S.; Long, D.-L.; Cronin, L.; McMillan, P. F. *J. Solid State Chem.* **2012**, *186*, 171.
(37) Long, D.-L.; Abbas, H.; Kögerler, P.; Cronin, L. *Angew. Chem., Int. Ed.* **2005**, *44*, 3415.
(38) Xin, F.; Pope, M. T. *J. Am. Chem. Soc.* **1996**, *118*, 7731.
(39) Botar, A.; Botar, B.; Gili, P.; Müller, A.; Meyer, J.; Bögge, H.; Schmidtmann, M. *Z. Anorg. Allg. Chem.* **1996**, *622*, 1435.
(40) Khoshnavazi, R.; Bahrami, L. *J. Coord. Chem.* **2009**, *62*, 2067.
(41) Krebs, B.; Droste, E.; Piepenbrink, M.; Vollmer, G. *C. R. Acad. Sci., Ser. IIc: Chim.* **2000**, *3*, 205.
(42) Sokolov, M. N.; Izarova, N. V.; Virovets, A. V.; Fedin, V. P.; Starikova, Z. A.; Antipin, M. Y. *Dalton Trans.* **2003**, 4389.
(43) Zhang, Z.; Lin, Q.; Zheng, S.-T.; Bu, X.; Feng, P. *Chem. Commun.* **2011**, *47*, 3918.
(44) Tézé, A.; Hervé, G. *J. Inorg. Nucl. Chem.* **1977**, *39*, 2151.
(45) Tézé, A.; Hervé, G. *J. Inorg. Nucl. Chem.* **1977**, *39*, 999.
(46) *SAINT*; Bruker AXS, Inc.: Madison, WI, 2009.
(47) *SADABS*; Bruker AXS, Inc.: Madison, WI, 2008.
(48) *SHELXTL-97*; Bruker AXS, Inc.: Madison, WI, 2003.
(49) Zhao, C.; Huang, Z.; Rodríguez-Córdoba, W.; Kambara, C. S.; O'Halloran, K. P.; Hardcastle, K. I.; Musaev, D. G.; Lian, T.; Hill, C. L. *J. Am. Chem. Soc.* **2011**, *133*, 20134.

(50) Glass, E. N.; Fielden, J.; Kaledin, A. L.; Musaev, D. G.; Lian, T.; Hill, C. L. *Chem.—Eur. J.* **2014**, *20*, 4297.
(51) Zhao, Y.; Truhlar, D. G. *Theor. Chem. Acc.* **2008**, *120*, 215.
(52) Hay, P. J.; Wadt, W. R. *J. Chem. Phys.* **1985**, *82*, 270.
(53) Wadt, W. R.; Hay, P. J. *J. Chem. Phys.* **1985**, *82*, 284.
(54) Hay, P. J.; Wadt, W. R. *J. Chem. Phys.* **1985**, *82*, 299.
(55) Tomasi, J.; Persico, M. *Chem. Rev.* **1994**, 2027.
(56) Cammi, R.; Tomasi, J. *J. Comput. Chem.* **1995**, *16*, 1449.
(57) Rappe, A. K.; Casewit, C. J.; Colwell, K. S.; Goddard, W. A.; Skiff, W. M. *J. Am. Chem. Soc.* **1992**, *114*, 10024.
(58) Frisch, M. J.; Trucks, G. W.; Schlegel, H. B.; Scuseria, G. E.; Robb, M. A.; Cheeseman, J. R.; Scalmani, G.; Barone, V.; Mennucci, B.; Petersson, G. A.; Nakatsuji, H.; Caricato, M.; Li, X.; Hratchian, H. P.; Izmaylov, A. F.; Bloino, J.; Zheng, G.; Sonnenberg, J. L.; Hada, M.; Ehara, M.; Toyota, K.; Fukuda, R.; Hasegawa, J.; Ishida, M.; Nakajima, T.; Honda, Y.; Kitao, O.; Nakai, H.; Vreven, T.; Montgomery, J. A.; , J.; Peralta, J. E.; Ogliaro, F.; Bearpark, M.; Heyd, J. J.; Brothers, E.; Kudin, K. N.; Staroverov, V. N.; Kobayashi, R.; Normand, J.; Raghavachari, K.; Rendell, A.; Burant, J. C.; Iyengar, S. S.; Tomasi, J.; Cossi, M.; N. Rega, J. M. M.; Klene, M.; Knox, J. E.; Cross, J. B.; Bakken, V.; Adamo, C.; Jaramillo, J.; Gomperts, R.; Stratmann, R. E.; Yazyev, O.; Austin, A. J.; Cammi, R.; Pomelli, C.; Ochterski, J. W.; Martin, R. L.; K. Morokuma, V. G. Z.; Voth, G. A.; Salvador, P.; Dannenberg, J. J.; Dapprich, S.; Daniels, A. D.; Ö. Farkas, J. B. F.; Ortiz, J. V.; Cioslowski, J.; Fox, D. J. *Gaussian 09*, Revision C.01; Gaussian, Inc.: Wallingford, CT, 2009.
(59) Spek, A. L. *J. Appl. Crystallogr.* **2003**, *36*, 7.
(60) Alcock, N. W.; Pennington, M.; Willey, G. R. *J. Chem. Soc., Dalton Trans.* **1985**, 2683.
(61) Veith, M.; Wolfanger, H.; Huch, V. *Z. Naturforsch., B: Chem. Sci.* **1995**, *50*, 1130.
(62) Zhao, C.; Rodríguez-Córdoba, W.; Kaledin, A. L.; Yang, Y.; Geletii, Y. V.; Lian, T.; Musaev, D. G.; Hill, C. L. *Inorg. Chem.* **2013**, *52*, 13490.
(63) Takashima, T.; Yamaguchi, A.; Hashimoto, K.; Nakamura, R. *Chem. Commun.* **2012**, *48*, 2964.
(64) Kudo, A.; Kato, H.; Nakagawa, S. *J. Phys. Chem. B* **2000**, *104*, 571.
(65) Miseki, Y.; Kudo, A. *ChemSusChem* **2011**, *4*, 245.
(66) Zhang, Z.; Lin, Q.; Kurunthu, D.; Wu, T.; Zuo, F.; Zheng, S.-T.; Bardeen, C. J.; Bu, X.; Feng, P. *J. Am. Chem. Soc.* **2011**, *133*, 6934.
(67) Kortz, U.; Savelieff, M. G.; Bassil, B. S.; Keita, B.; Nadjo, L. *Inorg. Chem.* **2002**, *41*, 783.
(68) Bi, L.-H.; Li, B.; Bi, S.; Wu, L.-X. *J. Solid State Chem.* **2009**, *182*, 1401.
(69) Pope, M. T.; Varga, G. M. *Inorg. Chem.* **1966**, *5*, 1249.
(70) Kozik, M.; Hammer, C. F.; Baker, L. C. W. *J. Am. Chem. Soc.* **1986**, *108*, 7627.
(71) Yamase, T. *Chem. Rev.* **1998**, *98*, 307.
(72) Long, D.-L.; Kögerler, P.; Cronin, L. *Angew. Chem., Int. Ed.* **2004**, *43*, 1817.
(73) Wang, J.-P.; Ma, P.-T.; Li, J.; Niu, H.-Y.; Niu, J.-Y. *Chem.—Asian J.* **2008**, *3*, 822.
(74) Zhao, C. Ph.D. thesis, Emory University, 2013.
(75) Nalin, M.; Messaddeq, Y.; Ribeiro, S. J. L.; Poulain, M.; Briois, V.; Brunklaus, G.; Rosenhahn, C.; Mosel, B. D.; Eckert, H. *J. Mater. Chem.* **2004**, *14*, 3398.
(76) Balula, S. S.; Granadeiro, C. M.; Barbosa, A. D. S.; Santos, I. C. M. S.; Cunha-Silva, L. *Catal. Today* **2013**, *210*, 142.
(77) Keyes, T. E.; Gicquel, E.; Guerin, L.; Forster, R. J.; Hultgren, V.; Bond, A. M.; Wedd, A. G. *Inorg. Chem.* **2003**, *42*, 7897.
(78) Stowe, A. C.; Nellutla, S.; Dalal, N. S.; Kortz, U. *Eur. J. Inorg. Chem.* **2004**, 3792.
(79) Mbomekalle, I.-M.; Lopez, X.; Poblet, J. M.; Secheresse, F.; Keita, B.; Nadjo, L. *Inorg. Chem.* **2010**, *49*, 7001.
(80) Kuznetsov, A. E.; Geletii, Y. V.; Hill, C. L.; Morokuma, K.; Musaev, D. G. *Theor. Chem. Acc.* **2011**, *130*, 197.
(81) Duncan, D. C.; Fox, M. A. *J. Phys. Chem. A* **1998**, *102*, 4559.
(82) Texier, I.; Delaire, J. A.; Giannotti, C. *Phys. Chem. Chem. Phys.* **2000**, *2*, 1205.
(83) Tanielian, C.; Seghrouchni, R.; Schweitzer, C. *J. Phys. Chem. A* **2003**, *107*, 1102.